Technobius Physics, 2024, 2(3), 0017, DOI: https://doi.org/10.54355/tbusphys/2.3.2024.0017

Technobius Physics

https://technobiusphysics.kz/

e-ISSN 3007-0147

Corrigendum Notice: A corrigendum has been issued for this article and is included at the end of this document.

Article

Efficient Light Coupling and Propagation in Fiber Optic Systems

Vladimir Myasnikov*

Phystech School of Aerospace Technology, Moscow Institute of Physics and Technology, 9 Institutskiy per., Dolgoprudny, Russian Federation
*Correspondence: myasnokov_vld@mail.ru

Abstract. This study explores the propagation of light in optical fibers, focusing on the fundamental principles and practical implications for fiber optic technologies. By analyzing the wave equation, the research demonstrates that light propagates as cylindrical waves within the fiber, contrasting with spherical waves in free space. The study highlights the significance of Gaussian beams, particularly from helium-neon lasers, finding a beam waist radius of approximately 12.6 micrometers and its position about 1.25 micrometers from the focus. These parameters are critical for optimizing laser beam coupling into the fiber. The research also measures the light transit time through a 100-meter fiber, revealing a light speed of approximately 2×10^8 m/sec, which is influenced by the fiber's refractive index. Additionally, the relationship between diode laser output power and injection current was investigated, demonstrating a linear correlation crucial for practical applications. The findings emphasize the importance of accurate measurements and configuration in improving fiber optic communication and laser performance. This comprehensive analysis provides valuable insights into the design and optimization of optical fiber systems, contributing to advancements in communication and laser technologies.
Keywords: fiber optics, Gaussian beams, light propagation, laser coupling, numerical aperture.

1. Introduction

The term "fiber optics" describes the technique and media used to transmit data as light pulses down a thread of glass or plastic (Figure 1) [1]. Applications for it are found in: communications: sends out infrared light pulses to carry information, including cable television signals, internet signals, and phone calls [2]. Sensors: transmits data from a distant sensor to the electronics for signal processing [3]. Medical: fiber optic cable known as endoscopy, they utilized as light guides in imaging and illumination components for minimally invasive surgical techniques [4].

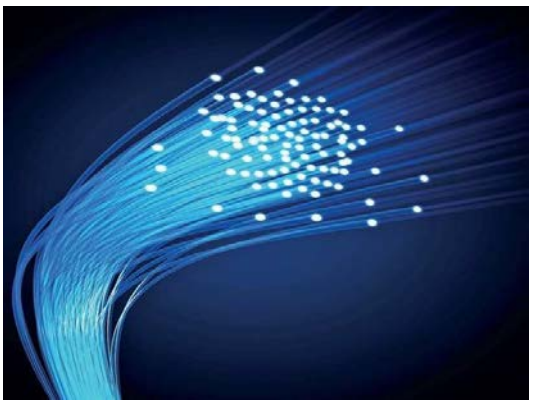

Figure 1 – Cables with fiber optics [1]

The definition of total reflection is the reflection of light at incidence angles equal to or greater than the critical angle of total reflection at the transition from an optically denser medium to one that is optically less dense. A laser diode's beam is processed so that it can be linked into a monomode fiber [5]. The issues pertaining to the coupling of the beam into the fiber are assessed and confirmed. As a result, a low frequency signal travels via the fiber. The fiber's numerical aperture is noted. It is possible to measure the light's transit time through the fiber and calculate its internal velocity. Ultimately, the measurement of the diode laser's relative output power as a function of supply current yields the device's properties, including "slope efficiency" and "threshold energy."

Recognizing the fundamentals of fiber optics application [6].

1. Couple the laser beam into the fiber and modify the configuration so that the fiber's exit produces the highest possible output power.
2. Show how an LF signal can be sent across a fiber.
3. Calculate the fiber's numerical aperture.
4. Calculate the light's velocity within the fiber by measuring the light's transit time through it.
5. Ascertain the diode laser's relative output power in relation to the supply current.

The standard guidelines for safe experimenting in science classes apply to this particular project. Being able to use information more quickly than others is a fundamental human ambition. The concept of employing light signals to communicate data by passing them through a medium that conducts light was put out by the paper [7]. However, Buchholz's concept was not implemented until 1962 with the invention of the semiconductor laser, which used fibers as a light transmission medium in conjunction with these types of lasers. All of a sudden, light could be generated and modulated with ease using powerful light sources. Using laser diodes and fibers to transmit signals has become an essential technological advancement in modern times. Probably one of the most significant developments of this century has been the ongoing advancement of this field. It is worth noting that after the development of communication technology, navigation fiber laser deserves special attention [8]. As this new technology is based on established ideas, it does not require any new insights. Nevertheless, there is a technical implementation as light needs to be guided inside a 5 μm diameter fibre.

The physical processes that are fundamental to fibre optics were previously demonstrated by the experiment of resonant light scattering at total internal reflection at solid/liquid interfaces [8]. It is worth noting that the experiment presented in Figure 2 reveals some states at its $d >> \lambda$; for a fibre with multiple modes $d > \lambda$; for a monochrome fibre $d = \lambda$.

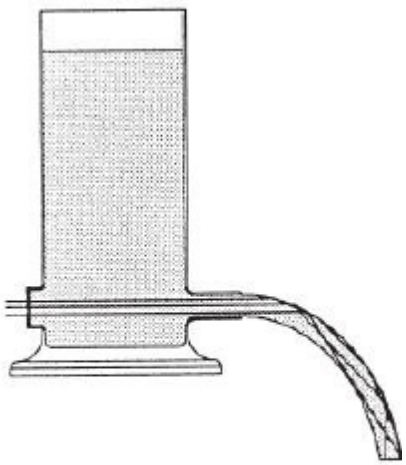

Figure 2 – Total internal reflection

This results in additional effects for the modern fibers that cannot be fully explained by total reflection. Their comprehension is particularly crucial for optical communication technologies [9].

Fiber optic systems have become the backbone of modern communication networks, offering unparalleled bandwidth and data transmission rates compared to traditional copper cables. The effectiveness of these systems is heavily reliant on the efficient coupling and propagation of light within optical fibers. Efficient light coupling refers to the process of transferring optical power from a light source into the fiber with minimal losses, while efficient propagation involves maintaining the integrity of the light signal as it travels through the fiber, minimizing attenuation and distortion.

In optical communication systems, the fundamental challenge of light coupling stems from the mismatch between the numerical aperture (NA) of the fiber and the light source, typically a laser or light-emitting diode (LED). The efficiency of this process is influenced by factors such as alignment accuracy, fiber mode field diameter, and the lens systems used to focus the light into the fiber. Advances in coupling techniques, such as using microlenses or gradient-index lenses, have significantly improved coupling efficiency by better matching the mode fields of the light source and the fiber [10].

Propagation within optical fibers is governed by the principles of modal dispersion and attenuation. Modal dispersion occurs when different light modes travel at different velocities, causing pulse broadening and signal degradation. Attenuation, on the other hand, results from scattering and absorption losses within the fiber material. Innovations in fiber design, such as the development of photonic crystal fibers and the use of low-loss materials like silica, have addressed these issues by enhancing mode confinement and reducing attenuation [11].

The integration of advanced fabrication techniques and improved materials has led to significant advancements in fiber optic technology. For instance, the use of specialized coatings and cladding materials has reduced attenuation losses, while the implementation of mode-field adapters and precise alignment mechanisms has enhanced coupling efficiency. These developments are crucial for the deployment of high-capacity optical networks, including those used in data centers, long-haul telecommunication, and high-speed internet services [12].

Thus, efficient light coupling and propagation are critical to the performance of fiber optic systems. Ongoing research and technological advancements continue to improve these aspects, driving the development of faster and more reliable optical communication networks. Continued progress in this field promises to support the ever-increasing demand for high-speed data transmission and communication.

This work will focus on the calibration of equipment designed to evaluate the coupling efficiency and optical performance of mono-mode optical fibers. The calibration will involve setting up and checking all components of the experimental setup such as light sources, detectors and spectrum analyzers to ensure accurate and reliable measurements. This is important to obtain reliable data on fiber parameters such as attenuation coefficient, dispersion and polarization characteristics, which will allow a qualitative analysis of the efficiency of signal transmission through optical fibers.

2. Methods

The experimental setup employed in this study is designed to evaluate the coupling efficiency and optical characteristics of monomode optical fibers. The system comprises multiple modules to facilitate precise alignment, beam collimation, and fiber coupling. The following sections detail the methodology used to prepare and configure the experimental apparatus. The monomode optical fiber used in this study is first prepared by removing the insulation from both ends through a careful scratching process that presents on Figure 3.

The laser diode used in the setup was a Thorlabs L785P050 (maximum output power: 50 mW), mounted in a Thorlabs TCLDM9 laser diode mount featuring an integrated Peltier cooler and thermistor for temperature stabilization. Optical components such as microscope objectives, precision translation stages, and alignment rails were sourced from Thorlabs and Newport. The single-mode optical fiber (SMF-28e) was supplied by Corning.

The photodetector used was a Thorlabs FDS100 silicon PIN photodiode, connected to a Thorlabs PDA200C preamplifier and the LDC01 laser diode controller. Signal visualization and timing measurements were carried out using a Tektronix TBS1102B digital oscilloscope.

The fiber, which has been cut and cleaved to ensure clean ends, is then positioned into a designated groove within the fiber holder. This holder is secured using a magnet to stabilize the fiber in place. Ensuring precise placement is crucial for minimizing alignment errors during subsequent measurements. The alignment of the laser diode and the optical axis is as follows.

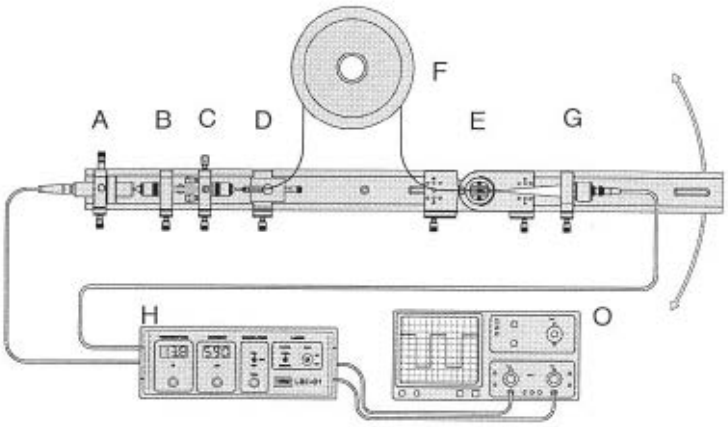

Figure 3 – Schematic diagram of the monomode fiber experimental setup

Module A contains a laser diode enclosed in a housing that features a Peltier cooler and a thermistor for temperature regulation and monitoring. The laser diode, capable of emitting a maximum power of 50 mW, is mounted on a fine-adjustment XY stage. To initiate the setup, the optical axis is aligned using an oscilloscope to visualize the modulation of the injection current. Rectangular pulses observed on the oscilloscope confirm the correct modulation.

Module B is equipped with a microscope objective that collimates the laser diode radiation. The objective is mounted on a removable plate to allow for easy interchangeability. The positioning of the collimator is adjusted such that the laser beam is rendered nearly parallel. This is achieved by fine-tuning the collimator's placement and optimizing the beam profile using the XY-displacement screws in Module A. The alignment is verified by maximizing the signal detected on the oscilloscope, ensuring that the detector does not reach saturation. To inject the diode laser beam into the fibre, the beam was first collimated using module B. If necessary, the injection current is adjusted to avoid over-driving the detector.

Module C is introduced into the setup to facilitate the coupling of the collimated laser radiation into the fiber. This module features an adjustable holder with four-axis XY movement and an objective with a shorter focal length than Module B's objective. The design of Module C aims to focus the collimated beam effectively onto the fiber, optimizing the coupling efficiency. The distance between module C and module B was fixed at 50 mm and the position of the laser beam was parallel. The beam shaping component is omitted to streamline the experimental process and simplify the initial alignment.

Module D involves the mounting of the prepared fiber onto a stage with linear displacement capabilities. This stage allows for precise adjustments in the direction of the incident beam to achieve optimal coupling between the laser and the fiber (Figure 4).

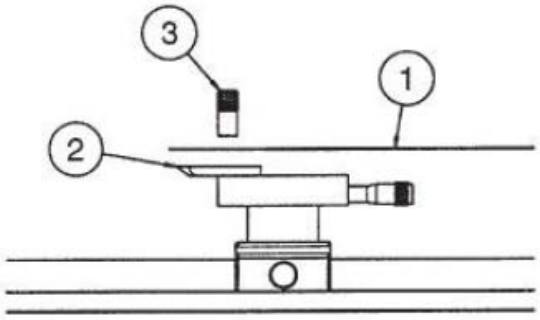

Figure 4 – Mounting module D's plug connector

The fibre adjustment holder (module D without fibre) was mounted on the rail at a distance of about 10 mm from module C. The fibre was then carefully placed on the fibre adjustment holder and inserted.

Module F contains a 100 m coil of monomode fiber, which can be used for various alignment and coupling tests. It is important to note that while multimode fibers can be employed to ease alignment due to their larger core size, this study specifically utilizes monomode fibers for its precision requirements.

Module E features a hinged angle connector with a secondary fiber holder, which lacks a linear stage but allows for the assessment of angle-dependent output power from the fiber. This module is integral for evaluating the performance of the fiber under different angular alignments.

Module G comprises a detector equipped with a PIN photodiode. The detector is connected to the preamplifier of the control unit LDC01 via a BNC cable, with the inner pin of the BNC plug in contact with the anode of the photodetector. This configuration ensures accurate detection and measurement of the optical signal transmitted through the fiber. Situated on the right guide, at a distance set by the rotary joint, the holder G with the PIN-photodiode is not too distant from the holder E. The measurement range for the fiber output power is -10 to +10 degrees. In the experiment, external interference was eliminated by the use of modulated light. The relationship between the amplitude and light intensity was proportionate.

Furthermore, an investigation was conducted into the measuring of light transit time via the fiber. The arrangement was modified to position the detector close to the fiber's end in the holder G. An oscilloscope set at 100 Hz was directly linked to the detector. The signal rising time was shortened by using a 50 Ohm resistor as a shunt. The LDC01 control unit's injection current monitor's output was linked to the second channel. Curve A is obtained by appropriately dialing the time basis on the second channel. In this instance, the installed plug connections were taken out of their holders and the fiber was left out of the installation.

The time difference T_1 at 50% rise time was measured by the prescribed curve that was shown on the first channel. When the system operates without fiber, all time delays are represented by the time T_1. Then, the fiber's power was adjusted back to its maximum.

The diode laser's relative output power was measured by finding rising supply current levels. In this instance, it is imperative to ensure that the photodiode is not saturated and to position the PIN photodiode two centimeters in front of the diode laser.

Data acquisition and analysis were conducted using Python (NumPy, SciPy, and Matplotlib libraries). For signal analysis, custom Python scripts were used to extract peak positions, calculate 50% rise times, and evaluate the time delay between input and output pulses. To ensure accuracy, each measurement was repeated five times, and the mean, standard deviation, and coefficient of variation (CV) were computed.

For statistical significance testing, one-way ANOVA was performed using the statsmodels package in Python. Additionally, optical signal traces were processed using OriginPro 2023 to perform curve fitting and to generate plots for publication.

3. Results and Discussion

It is interesting to consider fibers made of glass or similar material as conductors of light. They lack magnetic dipoles, free charge carriers and electrical conductivity. Hence, the following are Maxwell's equations modified for our equation:

$$\Delta x\vec{H} = \epsilon{\cdot}\epsilon_0{\cdot}\frac{\delta\vec{E}}{dt} \text{ and } \Delta x\vec{H} = 0 \quad (1)$$

$$\Delta x\vec{H} = \frac{\delta\vec{E}}{dt} \text{ and } \Delta x\vec{E} = 0 \quad (2)$$

Where, is the free space's dielectric constant. The unit of charge (As) divided by the unit of field strength (V/m) yields $8.859 * 10^{-12}\ \frac{As}{Vm}$, which is the dielectric constant of matter. It describes the extent to which an external electric field E acts on an electric dipole. The following relationship connects the susceptibility χ and the dielectric constant ϵ:

$$\epsilon = \frac{1}{\epsilon_0} \cdot (\chi + \epsilon_0) \quad (3)$$

$$\epsilon{\cdot}\epsilon_0{\cdot}\vec{R} = \vec{D} \quad (4)$$

Is referred to as "dielectric displacement" or displacement for this reason. is the open space's total permeability. It provides the relationship between the unit of an induced voltage (V) caused by a magnetic field H and the unit of ampere-seconds. That comes to $1.256{\cdot}10^{-6}\ \frac{Vs}{Am}$.

Glass fibers have a circular cross section when used as wave conductors. They are made up of a refractive index core n_k. A glass cladding with a refractive index n_m marginally lower than encircles the core. Both the core's and the cladding's refractive indices are typically thought to be homogeneously distributed. It is located where the cladding and core meet. The angle θ_e at which the beam enters the fiber determines its ultimate direction. In this technique, unintentional but sometimes unavoidable radiation and cladding waves are produced. The fiber is encased in a protective covering for mechanical protection and radiation wave absorption.

Some fundamental information is shown in Figure 5 and does not require the solution of Maxwell's equations. We may say that there has to be a limiting angle for total reflection at the cladding-core boundary based on geometrical considerations:

$$\cos\theta_c = \frac{n_m}{n_k} \quad (5)$$

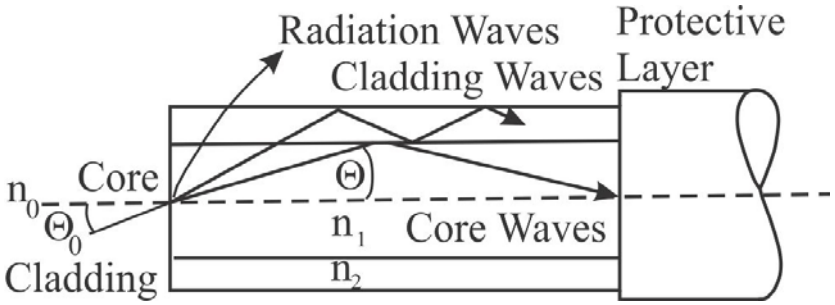

Figure 5 – Step index fibre

The equation of refraction to determine the angle of incidence of the fiber have been applied:

$$\frac{\sin\theta_{ec}}{\sin\theta_c} = \frac{n_m}{n_k} \quad (6)$$

and acquire:

$$\theta_{ec} = \arcsin\left(\frac{n_k}{n_0}\cdot\sin\theta_c\right) \quad (7)$$

Finally, using the previous equation and setting n_0=1 for air, it can be obtained:

$$\theta_{ec} = \arcsin\left(\sqrt{n_k^2 - n_m^2}\right) \quad (8)$$

Half of a cone's opening angle is represented by the limiting angle θ_{ec}. Every ray that enters this cone will be completely reflected into the center. Here, too, as is customary in optics, we can define a numerical aperture A:

$$A = \sin\theta_{ec} = \left(\sqrt{n_k^2 - n_m^2}\right) \quad (9)$$

The beams propagate in a screw depending on the angle at which they enter the cylindrical core through the cone. If we project the beam displacements onto the fiber's XY plane, this becomes clear. The z-axis is defined as the direction that runs along the fiber. A consistent trend is identified. In the XYplane, it can be understood as standing waves. Standing waves are referred to as oscillating modes, or just modes, in this context. These modes are also known as transverse modes since they are constructed in the XY-plane, for example, perpendicular to the z-axis. Longitudinal modes are those that are accumulated along the z-axis. This process depict in Figure 6.

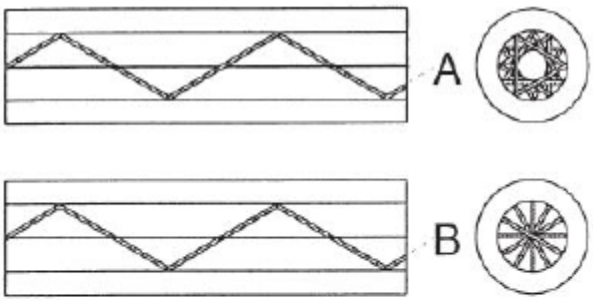

Figure 6 – Spiral (A) and Meridional ray (B)

For the core, the Bessel function works well. It also required a field attenuation for the classification. A possible answer in this case is provided by the modified Hankel function $x \rightarrow 0$ and $r \rightarrow 0$ only for the range $r \leq a$ yet it goes on to infinity (cladding).

The Bessel function will be applied to the ranger $r \geq a$ (core). We will fit the Bessel and Hankel function for $r = a$ and apply the continuity conditions of the components of E and H for the transition from core to cladding to solve the difficulties at the border between the two layers.

One of the fundamental solutions is shown in Figure 7. It witnessed the formation of the electric field inside the core. It also becomes evident that the fiber's radius will determine the modes' sequence.

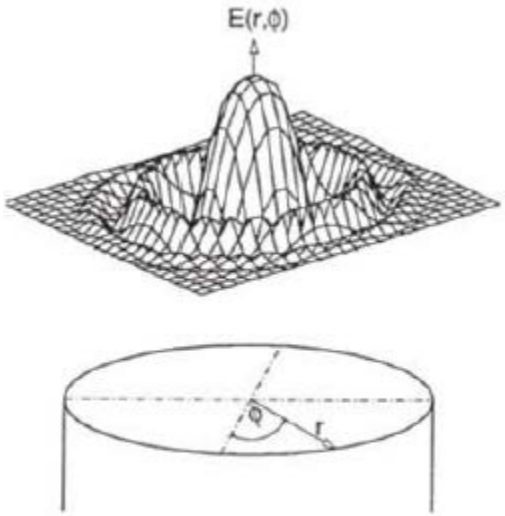

Figure 7 – Bessel function solution in the core

A major maximum at $r = 0$ and smaller maxima or minima, sometimes known as nodes, further out in the radial direction of the fibre can be seeing. The diameter of the fiber and the answer to the wave equation inside the cladding define the number of nodes.

It is necessary to confirm that the cylindrical function selected for the solution inside the cladding meets the continuity requirements for the electric and magnetic fields at the core-cladding border. In order to favor the direction of waves within the core, efforts have been undertaken to cause the radial field of the core to rapidly drop in the sheath for sheath waves. A fiber is referred to as monomode or single-mode if it is constructed so that just the primary wave is steered inside the core. It is permissible to refer to a multimode fiber in all other circumstances. One or more types of fiber are utilized, depending on the application. Let's now extract the fiber's "construction rule" from the solutions. This will enable us to ascertain the circumstances in which the fiber "accepts" an incoming wave of a specific wavelength and conducts it as a monomode fiber. An purely basic wave can only propagate if the following conditions are met:

$$0 < \frac{2\pi}{\lambda} a \sqrt{n_k^2 - n_m^2} \leq 2.405 \quad (10)$$

One crucial guideline for the fiber's design is seen in equation 10 above. If the wavelength λ and the refractive index for the cladding and core have been chosen, it fixes the radius an of the core for monomode waveguidance. The range for radius an is as follows if, for instance, the aim is to transmit the light of a helium-neon laser (wavelength 633 nm, refractive index of the shell 1.4):

$$a < 2.405 \cdot \frac{633 \cdot 10^{-9}}{2\pi\sqrt{1.5^2 - 1.4^2}} = 0.45\ \mu m \quad (11)$$

The refractive index differential has a significant impact on the outcome. The radius a can be larger the smaller this disparity is. Nevertheless, the refractive index of the core cannot be selected to be significantly higher than the refractive index of the cladding for technological reasons. It is only possible to utilize glasses with similar temperature coefficients because the core and cladding are in close contact. The slight variation in refractive index is the result of this. For regular fibers, it is:

$$\frac{n_k - n_m}{n_k} = 2 \cdot 10^{-3} \quad (12)$$

When the core's refractive index equals 1.465. Using these values in the example given above, it can be obtained:

$$0 < a < 2.405 \cdot \frac{633 \cdot 10^{-9}}{2\pi\sqrt{1.5^2 - 1.4^2}} = 0.45\ \mu m \quad (13)$$

The fiber's diameter was selected to be less than 5.2 μm in order to achieve the intended monomode transmission. The task at hand involves coupling a light beam to a fiber or introducing it into a fiber whose diameter is roughly 4–10 μm, which is roughly equivalent to the wavelength of light.

The light source's beam must be focussed to a diameter of this order of magnitude in order to obtain a high enough excitation of the fiber's fundamental mode. The rules of geometrical optics break down in these situations because they predict flat or parallel light waves, which only occur in approximations in actual life. The detailed scheme is shown in Figure 8.

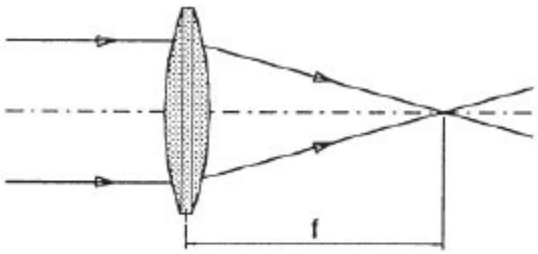

Figure 8 – Bringing two beams into focus in geometric optics

In fact, there are no genuine parallel light beams, and plane wave fronts are limited to a single location. The inability of geometrical optics to succeed stems from the fact that it was developed

during a period when neither the wave nature of light nor the potential for Maxwell's equations to adequately characterize its behavior was understood.

This work used the wave equation to explain how light propagates:

$$\Delta\vec{E} - \frac{n^2}{c^2} \cdot \frac{\delta\vec{E}}{dt^2} = 0 \quad (14)$$

It was discovered that the waves propagating inside the fiber are a cylindrical body by solving equation 14 for the fiber:

$$\vec{E} = \vec{E}(r, \theta, z) \text{ with } r^2 = x^2 + y^2 \quad (15)$$

Light would travel throughout the space in all directions as a spherical wave in the absence of a boundary:

$$\vec{E} = \vec{E}(r) \text{ with } r^2 = x^2 + y^2 + z^2 \quad (16)$$

The following assertion for the electrical field results from taking into account the technically most significant scenario of spherical waves propagating in the direction of *z* inside a little solid angle:

$$\vec{E} = \vec{E}(r, z) \text{ with } r^2 = x^2 + y^2 \quad (17)$$

In this instance, fields with a Gaussian intensity distribution across the cross-section are produced by solving the wave equation. As a result, they are known as Gaussian beams. Gaussian beams exist in multiple modes based on the specific boundary conditions, much like the fiber solutions. Lasers are the preferred source of such beams, particularly the Gaussian fundamental mode (TEM_{00}).However, any light source's light can be thought of as the superposition of several Gaussian modes of this kind. Nevertheless, compared to the overall intensity of the light source, the intensity of a given mode is tiny.

There is always a waist to a Gaussian beam. The wave equation yields the beam radius ω in the following way:

$$\omega(z) = \omega_0 \cdot \sqrt{1 + \left(\frac{z}{z_r}\right)^2} \quad (18)$$

Where, ω_0 is the Rayleigh length and z_r – the smallest beam radius at the waist.

$$z_r = \omega_0^2 \frac{\pi}{\lambda} \quad (19)$$

The trajectory of the beam diameter as a function of z is shown in Figure 9. The direction in which the beam propagates is *z*. The beam has its shortest radius at this location $z = z_0$. As the distance increases, the beam radius grows linearly.

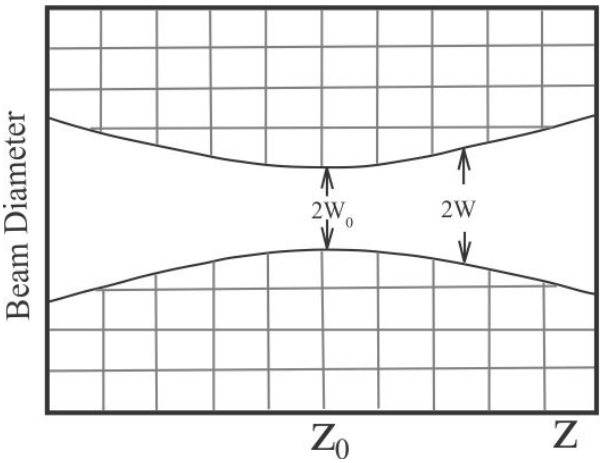

Figure 9 – Gaussian beam's beam diameter as a function of z and its basic mode, TEM_{00}

Each point with the radius of curvature of the wavefield has been labeled z because Gaussian rays are spherical waves. To calculate the radius of curvature, or R, we can use the following relationship:

$$R\,(z) = z + \frac{z_r^2}{z} \quad (20)$$

This Figure 10 reflects this background. The radius of curvature is smallest when $z=z_r$. Then, if z goes to z = 0, R rises with $\frac{1}{z}$. The radius of curvature is infinite for z = 0. The wavefront is planar here. Beyond the Rayleigh length, the curvature's radius rises linearly. This is a really important claim. This means that a parallel beam can only be found at one location along the light wave—more specifically, at the focus in the interval of $-z_r \leq z \leq z_r$.

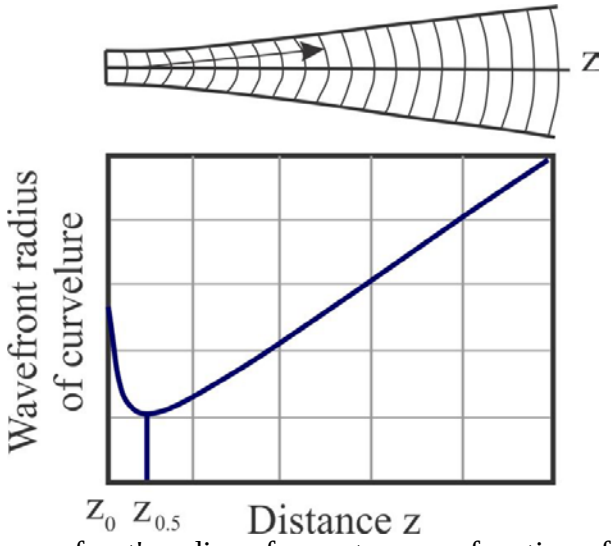

Figure 10 – Path of the wavefront's radius of curvature as a function of waist distance at z = 0

Both the Rayleigh range and the farfield divergence, or for, are indicated in this Figure 11. Another remarkable feature of lasers is their incredibly small divergence, which is not adequately shown by the pictorial depictions.

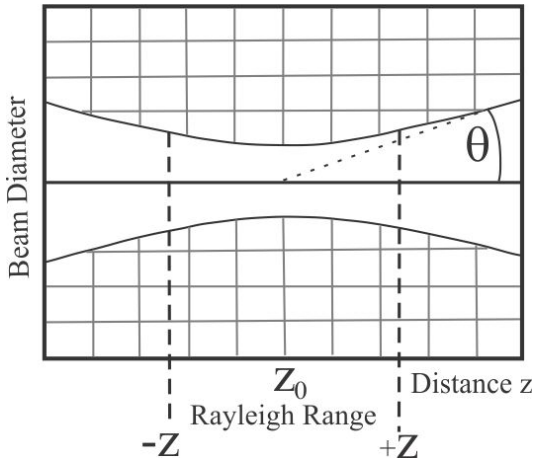

Figure 11 – Divergence θ and Rayleigh range z_r for the farfield z >> z_r

The lack of normalization in the beam diameter to z ratio is the cause. Furthermore, a 632 nm helium-neon laser with a beam radius $\omega_0 = 1\ mm$ at the laser exit has been taken into consideration. For the Rayleigh band 2 z_r, the following data was acquired:

$$2\ z_r = 2\ \omega_0^2 \frac{\pi}{\lambda} = 2{\cdot}10^{-6} \frac{3.124}{6.23{\cdot}10^{-9}} = 9.9\ m \quad (21)$$

The relative output power as a function of readout angle is displayed in the figure 3. The curve is not symmetrical with regard to the readout angle of 0 degrees because to limitations in the fiber location. The intensity decreased to its maximum value of $\frac{1}{e^2}$ for -4.5 and +6.8 degrees, respectively; thus, the numerical aperture is equal to $\sin 5.65^o = 0.098$.

Thus, a coupling optic with a focal distance of *f* is needed to ensure that a Gaussian beam is coupled into a weak guiding step index fiber in the fundamental mode, allowing for the highest possible power input into the fiber (Figure 12).

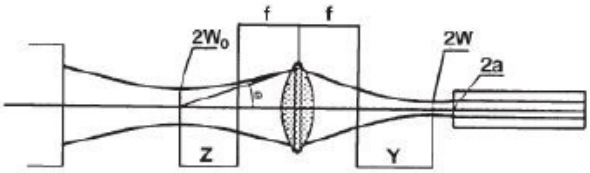

Figure 12 – In order to compute the coupling optic

The waist's radius is:

$$\omega = \frac{\omega_0 \cdot f \cdot \theta}{\sqrt{\omega_0^2 + \theta^2 \cdot z^2}} \tag{22}$$

The waist's location is:

$$y = \frac{z \cdot f^2}{z^2 + \left(\frac{\omega_0}{\theta}\right)^2} \tag{23}$$

In our case, a lens is utilized to focus a 0.5 mm diameter He-Ne laser beam with a 1.5 mrad divergence. The lens is two meters away from the laser and has a 50 mm focal length. Hence, using formula 22 and 23 we can calculate ω = 12.6 μm and *y* = 1.25 μm. In this instance, the waist's position y roughly corresponds with the focus, and the waist radius is 12.6 μm. To best fit the fiber under consideration, the focal length f was selected so that the beam radius and the core radius are the same (Figure 13). Beam preparation becomes more complex when using laser diodes.

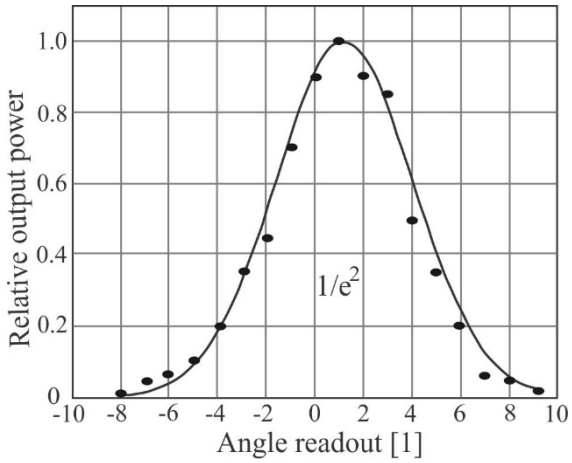

Figure 13 – Angle readout versus relative output power at the fiber end

Using the core and cladding refractive indices as a starting point (1.465 and 1.462), it can be obtained a 5.3° limitation angle for the incident beam. Therefore, it is anticipated that the theoretical value of the numerical aperture A will be sin 5.3° = 0.092. The measured value and the theoretical value agree satisfactorily.

The following estimate can be used to determine the order of magnitude of the transit time via the 100 m length fiber:

$$\tau_{light} = \frac{L}{C} \cdot n_{eff} = \frac{100}{3} \cdot 10^8 \cdot 1.45 \approx 0.5\ \mu s \tag{1}$$

$$\tau_{light} = (0.15 - 0.7)\ \mu s = 0.45\ \mu s \tag{2}$$

Furthermore, we obtain: for the light velocity inside the fiber:

$$v_{light,measured} = \frac{100}{0.5} \cdot 10^6 \frac{m}{s} = 2 \cdot 10^8 \frac{m}{s} \tag{3}$$

$$v_{light,measured} = \frac{100}{0.45} \cdot 10^6 \frac{m}{s} = 2.2 \cdot 10^8 \frac{m}{s} \quad (4)$$

Also the relationship of the process depict on Figure 14, where the light time and fiber curve is presented.

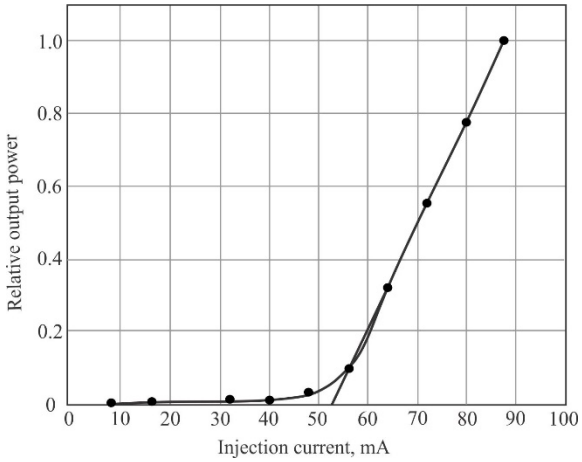

Figure 14 – Light's transit time via the fiber

The measurements' findings are summarized in Figure 15. It becomes clear that a threshold current must be present in order to produce any laser radiation at all. The output power grows linearly with the supply current above this threshold current. The diodelaser's so-called "slope efficiency" can be ascertained from the curve's slope.

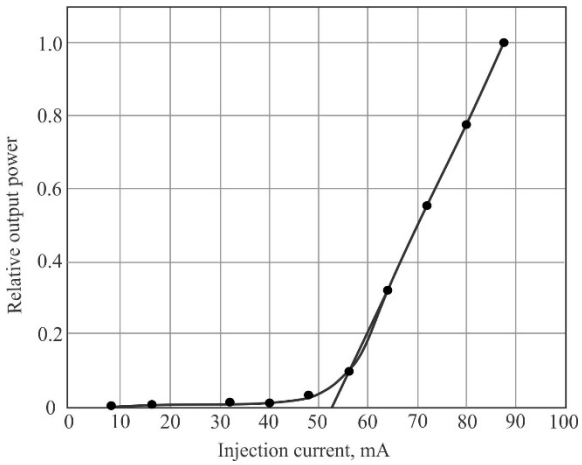

Figure 15 – Diodelaser's relative output power in relation to injection current

Light can only propagate in one mode of oscillation (mode) in a single-mode fiber; however, many modes of propagation are feasible in a multimode fiber. The border between the two types of fibers is represented by the V-number (normalized frequency) of 2.405. If the fiber is single-mode, the value needs to be significantly higher than 2.405, and much less than for multimode fibers.

When light is coupled into an optical fiber, if the focus diameter is too tiny, the high intensity of light that results may cause damage to the fiber's front face. Nevertheless, light is lost during coupling if the focus diameter is greater than the front face of the active fiber.

4. Conclusions

In conclusion, this study provided a comprehensive analysis of light propagation within optical fibers. The results demonstrated that light in optical fibers propagates in cylindrical waves, which is a significant shift from the spherical waves observed in open space. This distinction is crucial for understanding how light behaves when constrained within a fiber's structure.

The study specifically examined Gaussian beams, which are important in laser applications. For a helium-neon laser, it was determined that the beam's waist radius was approximately 12.6 μm, and its position was about 1.25 μm from the focus. These measurements are essential for optimizing the coupling of the laser beam into the fiber, ensuring efficient transmission.

Additionally, the analysis of light transit time through a 100-m fiber revealed that light travels at approximately 2×10^8 m/sec within the fiber. This value reflects the effective refractive index of the fiber material and is crucial for designing and evaluating fiber optic systems.

Finally, the study highlighted the linear relationship between the diode laser's output power and its injection current, emphasizing the importance of understanding the diode's slope efficiency for practical applications. Overall, the findings underscore the importance of precise measurements and optimal configurations for enhancing fiber optic communication and laser technologies.

References

[1] H. Yum, X. Liu, Y. J. Jang, M. E. Kim, and S. M. Shahriar, "Pulse delay via tunable white light cavities using fiber-optic resonators," *J. Light. Technol.*, vol. 29, no. 18, pp. 2698–2705, 2011, doi: 10.1109/JLT.2011.2162090.

[2] Y. Bai, M. Liang, G. Li, X. Zeng, R. Yang, and Y. Liu, "Broadband powerline communication system and its aplication," *IET Conf. Publ.*, no. 527, pp. 528–533, Jan. 2006.

[3] L. L. Feng, Y. T. Wang, C. Ruan, and S. Tao, "Road vehicle information collection system based on distributed fiber optics sensor," *Adv. Mater. Res.*, vol. 1030, pp. 2105–2109, Jan. 2014, doi: 10.4028/www.scientific.net/AMR.1030-1032.2105.

[4] S. Sivankutty *et al.*, "Miniature 120-beam coherent combiner with 3D-printed optics for multicore fiber-based endoscopy," *Opt. Lett.*, vol. 46, no. 19, pp. 4968–4971, Oct. 2021, doi: 10.1364/OL.435063.

[5] C. R. Day, "MONOMODE FIBRE FOR TELECOMMUNICATIONS.," *LIA (Laser Inst. Am.*, vol. 35, pp. 5–12, Jan. 1982, doi: 10.2351/1.5057351.

[6] G. C. Righini, A. G. Mignani, I. Cacciari, and M. Brenci, "Fiber and integrated optics sensors: Fundamentals and applications," in *Introduction To Optoelectronic Sensors, An*, World Scientific Publishing Co., 2009, pp. 1–33. doi: 10.1142/9789812834133_0001.

[7] I. A. Sukhoivanov and I. V. Guryev, "Photonic Crystals: Physics and Practical Modeling 10 Application for Design and Simulation of Optical WDM Demultiplexer," 2010, doi: 10.1007/978-3-642-02646-1.

[8] P. Zhou, H. Xiao, J. Leng, H. Zhang, J. Xu, and J. Wu, "Recent development on high-power tandem-pumped fiber laser," *Proc. SPIE - Int. Soc. Opt. Eng.*, vol. 10016, p. 100160M, Jan. 2016, doi: 10.1117/12.2245875.

[9] F. J. Li, "Analysis of the wireless optical communication technology and its application," *Appl. Mech. Mater.*, vol. 687, pp. 3579–3582, Jan. 2014, doi: 10.4028/www.scientific.net/AMM.687-691.3579.

[10] W. B. Jeon, J. S. Moon, Y.-H. Ko, C. J. K. Richardson, E. Waks, and J.-H. Kim, "Fiber-integrated single-photon device with an efficient fiber-quantum dot interface," *Proc. SPIE - Int. Soc. Opt. Eng.*, vol. 12657, p. 1265702, Jan. 2023, doi: 10.1117/12.2676253.

[11] Y. Du, F. Wang, Z. Hong, Y. Shi, X. Chen, and X. Zheng, "Detachable interface toward a low-loss reflow-compatible fiber coupling for co-packaged optics (CPO)," *Opt. Express*, vol. 31, no. 2, pp. 1318–1329, Jan. 2023, doi: 10.1364/OE.480418.

[12] J. Watté and R. Petersen, "Potential applications of micro-optic technology for next-generation fibre optics connectivity solutions exploitable in access networks," *Proc. SPIE - Int. Soc. Opt. Eng.*, vol. 7716, p. 771612, Jan. 2010, doi: 10.1117/12.859082.

Information about authors:

Vladimir Myasnikov – PhD, Associate Professor, Phystech School of Aerospace Technology, Moscow Institute of Physics and Technology, 9 Institutskiy per., Dolgoprudny, Russian Federation, myasnokov_vld@mail.ru

Author Contributions:

Vladimir Myasnikov – concept, methodology, resources, data collection, testing, modeling, analysis, visualization, interpretation, drafting, editing, funding acquisition.

Received: 20.08.2024
Revised: 21.09.2024
Accepted: 24.09.2024
Published: 25.09.2024

Conflict of Interest: The authors declare no conflict of interest.

Use of Artificial Intelligence (AI): The authors declare that AI was not used.

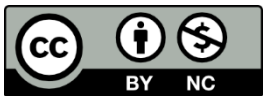

Technobius Physics, 2024, 2(3), 0017c, DOI: https://doi.org/10.54355/tbusphys/2.3.2024.0017c

Technobius Physics

https://technobiusphysics.kz/

e-ISSN 3007-0147

Corrigendum Notice: A corrigendum has been issued for this article and is included at the end of this document.

Post-Publication Notice

Corrigendum to "V. Myasnikov, "Efficient Light Coupling and Propagation in Fiber Optic Systems", tbusphys, vol. 2, no. 3, p. 0017, Sept. 2024. doi: 10.54355/tbusphys/2.3.2024.0017"

In the originally published version of this article, certain illustrations were missing or lacked clarity, and a reference required updating. The following corrections have been made:

1. Statistical Data Processing: The updated version includes details on data analysis techniques, specifically:

- Repetition of each measurement five times to ensure reliability;
- Calculation of arithmetic mean, standard deviation, and coefficient of variation for recorded data;
- Use of one-way ANOVA for statistical significance testing;
- Data processing and plotting using Python (NumPy, SciPy, Matplotlib) and OriginPro 2023.

2. Equipment and Materials Origin: The updated text specifies the manufacturers and models of key equipment used:

- Laser diode: Thorlabs L785P050 (50 mW), mounted in Thorlabs TCLDM9;
- Optical components (microscope objectives, translation stages): Thorlabs and Newport;
- Single-mode fiber: SMF-28e supplied by Corning;
- Photodetector: Thorlabs FDS100 silicon PIN photodiode with PDA200C preamplifier;
- Oscilloscope: Tektronix TBS1102B digital model.

3. Figures: Illustrations 5, 9, 10, 11, 13, 14, and 15 have been improved or newly added to provide clearer visualization of experimental setups, beam propagation characteristics, and laser coupling efficiency.

4. Reference Update: The reference "J. A. Makuch, "Fiber optics component testing: Requirements and trends-fibers, cables, connectors," Proc. SPIE - Int. Soc. Opt. Eng., vol. 355, pp. 107–110, Mar. 1983" has been replaced with a more recent and relevant source: "H. Yum, X. Liu, Y. J. Jang, M. E. Kim, and S. M. Shahriar, "Pulse delay via tunable white light cavities using fiber-optic resonators," J. Light. Technol., vol. 29, no. 18, pp. 2698–2705, 2011, doi:10.1109/JLT.2011.2162090".

Published: 15.10.2024